Chapter 2

Background

This chapter provides information relevant to the core parts of this research, with a particular focus on areas relevant to the novel work presented. We start by discussing the two main approaches to solving the NTE, Monte Carlo methods and deterministic methods, as the hybrid methods that are described next incorporate both types of solutions. Then, a discussion of previous work in the field of hybrid methods is given, with a specific focus on the CADIS method and variants on that method as well as significant historical work that has incorporated angular information into hybrid methods. Finally, we present a mathematical background for and derivation of the LDO equations.

2.1 Approaches to Solving the Neutron Transport Equation

2.1.1 Monte Carlo Methods

Solving the NTE using Monte Carlo methods approximates "following" the individual particles from birth to death. The purpose of particle tracking is to calculate the expectation or mean value $\bar{x}$ of some quantity of interest, often the neutron scalar flux. The estimate of this quantity takes the form of the average of N samples:

$$\hat{x} = \frac{1}{N} \sum_{n=1}^{N} x_n, \tag{2.1}$$

where x_n is the contribution from the n^{th} particle history to the quantity of interest. As the calculation proceeds, x_n is tallied from each neutron history in order to calculate the estimated or sample mean $\hat{x}$ at the end of the calculation. Errors in Monte Carlo calculations take the form of stochastic uncertainties, as the independent variables of the NTE are treated continuously. Taking this into consideration, it is useful to quantify how good of an estimate the sample value $\hat{x}$ is to the true mean value $\bar{x}$.

For some property of a Monte Carlo history x sampled from a continuous probability density function $f(x)$, the variance of that property is defined to be

$$\sigma^2(x) = \overline{x^2} - \bar{x}^2, \tag{2.2}$$

where

$$\overline{x^n} \equiv \int_{-\infty}^{\infty} x^n f(x) dx. \tag{2.3}$$

The standard deviation of the property is calculated as the square root of the variance:

$$\sigma(x) = \left(\overline{x^2} - \bar{x}^2\right)^{1/2} \tag{2.4}$$

and provides a measure of the spread of x about the mean value $\bar{x}$ [1]. With this, the variance and standard deviation of $\hat{x}$ can be expressed in terms of the variance and standard deviation of x as

$$\sigma^2(\hat{x}) = \frac{1}{N}\sigma^2(x) \tag{2.5}$$

and

$$\sigma(\hat{x}) = \frac{\sigma(x)}{\sqrt{N}}, \tag{2.6}$$

respectively. A low standard deviation indicates that the values of x are closely clustered near $\bar{x}$, while a high standard deviation indicates a large spread in the values of x. If $\hat{x}$, constructed from N values of x_n, is used to estimate $\bar{x}$, then the spread in the results of $\hat{x}$ about $\bar{x}$ is proportional to $\sigma(x)$ and falls off as the square root of the number of histories in the sample, as seen in Equation 2.6 [1]. This is to say, generally, that a greater number of histories contributing to the property of interest being calculated results in a lower standard deviation of the estimate of that property.

For a given Monte Carlo calculation, the sample variance is defined as

$$S^2 = \frac{1}{N-1}\sum_{n=1}^{N}(x_n - \hat{x})^2 \tag{2.7}$$

and is considered to be an unbiased estimator of the variance; the expectation value of the sample variance is equal to the variance, $\sigma^2(x)$ [1]. Because it is an unbiased estimator of the variance, the sample variance allows us to estimate the spread in $\hat{x}$; this is useful because $\hat{x}$ is the value that actually results from the Monte Carlo calculation. In practice, the sample variance and standard deviation are calculated as

$$S^2 = \frac{N}{N-1}\left(\widehat{x^2} - \hat{x}^2\right), \text{ where } \widehat{x^2} \equiv \frac{1}{N}\sum_{n=1}^{N} x_n^2, \tag{2.8}$$

and

$$S = \left(\frac{N}{N-1}\right)^{1/2} \left[\frac{1}{N}\sum_{n=1}^{N} x_n^2 - \hat{x}^2\right]^{1/2}, \tag{2.9}$$

respectively [1]. For large numbers of histories, $\frac{N}{N-1}$ is often set equal to one.

The simplest Monte Carlo model for particle transport problems is the "analog" model that uses the real probability that various events occur [2]. In the analog model, particles are followed from event to event, and the next event is always sampled from a number of possible events according to the real event probabilities. This is called the analog Monte Carlo model because it is directly analogous to the naturally occurring transport; it works well when a significant fraction of the particles contribute to the tally estimate and can be compared to detecting a significant fraction of the particles in the physical situation.

To quantify the efficiency of calculating a given quantity of interest, a metric known as the "figure of merit" is often used.

2.1.1.1 The Figure of Merit

The figure of merit (FOM) is defined as

$$\text{FOM} = \frac{1}{R^2 T}, \tag{2.10}$$

where R is the estimated relative error, defined as $S/\hat{x}$, and T is the computer time taken to complete the calculation [2]. This value should be approximately constant for any one Monte Carlo calculation, as R^2 is proportional to $1/N$ and T should be directly proportional to N.

As stated earlier, estimates for quantities of interest with the lowest statistical error are usually obtained for quantities to which a substantial fraction of the histories contribute. That is to say, in order to get estimates for quantities of interest that are statistically meaningful (have sufficiently low statistical error), a sizable number of the particle histories tracked should contribute to the estimate. This can be difficult to achieve in a reasonable amount of computational time for certain analog Monte Carlo calculations. That is to say, if these analog calculations were allowed to continue until convergence, they would have a very small FOM because of the sheer amount of calculation time needed for the calculation to finish. A pertinent example of this type of problem is a neutron shielding scenario, in which the neutron scalar flux varies by orders of magnitude through the shield and over the problem geometry. In these cases, "non-analog" techniques are introduced.

Non-analog Monte Carlo attempts to follow "interesting" particles more often than uninteresting ones, where an interesting particle is one that contributes much more to the quantity that needs to be estimated. Non-analog techniques are meant to increase the odds that a given particle contributes to the quantity of interest. To ensure that the average score

is the same in the non-analog model as in the analog model, the score is modified to remove the effect of biasing the natural odds.

A non-analog Monte Carlo technique will have the same expected tallies as an analog technique if the expected weight executing any given random walk is preserved. These variance reduction techniques can often decrease the relative error by sampling naturally rare events with an unnaturally high frequency and weighting the tallies appropriately. In the following subsection, several variance reduction methods are described and discussed.

2.1.1.2 Variance Reduction

Commonly used classes of variance reduction techniques are truncation methods, population control methods, and modified sampling methods [2]. Some variance reduction methods are generally applicable, while others are more specialized and carry high risk in use. Some variance reduction techniques cause an increase in computational time, but variance typically decreases faster than the increase in time, so these techniques still result in a net increase of the FOM [3].

Truncation Methods

Of the classes listed above, truncation methods are the simplest; they aim to accelerate calculations by truncating parts of phase space that do not contribute significantly to the problem solution. One example of this is geometry truncation, in which unimportant parts of the problem geometry are not modeled. Truncation methods may also be applied to other independent variables such as energy; when using energy cutoff, particles whose energy is out of the range of interest are terminated so that computation time is not spent following them.

Population Control Methods

Population control methods use particle splitting and Russian roulette to control the number of samples taken in various regions of phase space. In important regions, many samples of low weight particles are tracked, and in unimportant regions, few samples of high weight are tracked. Weight adjustments are made to the particles to ensure that the problem solution remains unbiased. Specific population control methods include geometry splitting and Russian roulette, energy splitting and roulette, weight cutoff, and weight windows [2].

Using geometry splitting with Russian roulette, particles transported from a region of higher importance to a region of lower importance undergo Russian roulette. Some of the particles will be killed a certain fraction of the time, but survivors will be counted more by increasing their weight the remaining fraction of the time. In doing this, unimportant particles are followed less often, yet the problem solution remains undistorted. If a particle is transported to a region of higher importance, it may be split into two or more particles, each with less weight and therefore counting less. In this case, important particles are followed

more often, yet the solution is again undistorted because, on average, the total weight is conserved.

In general, when a particle of weight w_0 is split into k particles, the resulting particles are each given a weight of $\frac{w_0}{k}$, conserving the expected weight. When a particle is subject to Russian rouletting, it is turned into a particle of weight $w_1 > w_0$ with probability $\frac{w_0}{w_1}$ and is killed with probability $1 - \frac{w_0}{w_1}$, again conserving the expected weight.

Geometry splitting with Russian roulette can be used to great advantage in deep penetration shielding problems. Splitting helps maintain the particle population, which diminishes rapidly in analog simulations. Conversely, geometry splitting with Russian roulette does not work well in problems that have severe angular dependence. In the most extremely anisotropic case, a particle may never enter a geometric region in which it may be split [2].

Energy splitting and Russian roulette are generally used in combination but may be employed separately. When using energy splitting, once a neutron drops below a given energy threshold, it may be split into multiple neutrons, each with an appropriately adjusted weight. This is useful when particles are more important in some energy ranges than in others. In the case of using energy rouletting, if a particle drops below a certain energy, a roulette game is played and the particle is either killed or survives with a weight increased by a factor of the reciprocal of the survival probability (to conserve overall particle population weight). These two energy-based variance reduction techniques are independent of spatial location, so a space-energy weight window (discussed below) is usually a better choice for problems with strong space-energy dependence.

When weight cutoff is employed, Russian roulette is played if a particle's weight drops below a specified cutoff value. The result of the roulette is that the particle is either killed or survives with its weight increased to a given level. Weight cutoff is most efficient when used in combination with geometry splitting (discussed above) and implicit capture (discussed below). It is important to note that, unlike in the case of the energy cutoff, the weight cutoff does not bias the solution because the particles that survive do so with increased weight.

The last population control method discussed here is the weight window, which is a phase space splitting and Russian roulette technique. The phase space may be space-energy or solely space. Each phase space cell is bounded by upper and lower weight bounds. If a particle is above the upper weight bound, it is split such that the resultant particles are all within the bounds of the weight window. If a particle is below the lower weight bound, Russian roulette is played and the particle is either terminated or permitted to survive with an increased weight within the bounds of the weight window. If a particle's weight is within the window, no action is taken. All of these scenarios are depicted in Figure 2.1, a cartoon of the weight window concept.

The weight window may be used alone to good effect, but it is particularly powerful when used in conjunction with other variance reduction techniques that introduce large variations in particle weight. Well-specified weight windows keep the Monte Carlo solution from severe perturbations resulting from high-weight particles and simultaneously keep computational resources from wasting time on low-weight particles by rouletting them.

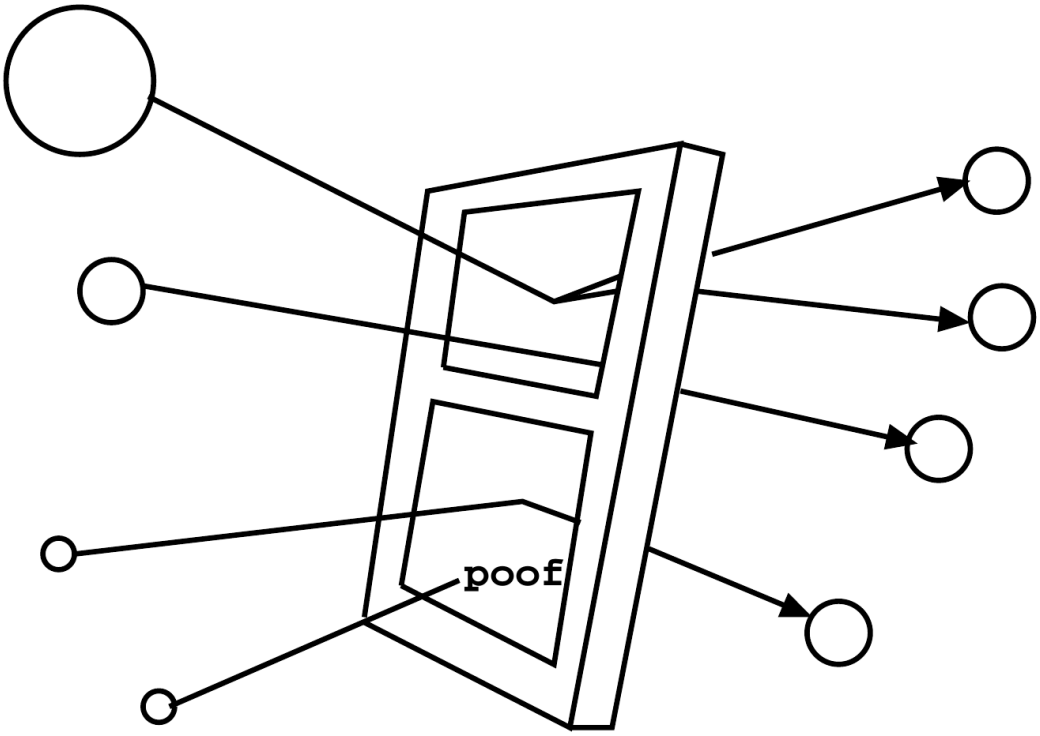

Figure 2.1: Weight window phase space splitting and Russian roulette [2].

Modified Sampling Methods

Modified sampling methods alter the statistical sampling of a problem to increase the number of tallies per particle. For a given Monte Carlo event, it is possible to sample from an arbitrary distribution rather than the physical probability as long as the particle weights are adjusted to compensate. With modified sampling methods, sampling is done from distributions that send particles in desired directions or into other desired regions of phase space such as time or energy. Modified sampling methods may also change the location or type of collisions. Categories of modified sampling methods include implicit capture, forced collisions, and source biasing.

Using implicit capture (also called implicit absorption or survival biasing), particles are never killed by absorption. Instead, a particle's weight is reduced by the absorption probability at each collision, allowing important particles to survive by not being lost to absorption. Implicit capture can be thought of as a splitting process in which a particle of weight w_0 is split into two particles: one of weight $w_0(1 - \frac{\Sigma_a}{\Sigma_t})$ that survives and is subsequently followed, and one of weight $w_0 \frac{\Sigma_a}{\Sigma_t}$ that is instantaneously killed [2].

The forced collision method increases sampling of collisions in specified spatial cells. Particles undergoing forced collisions are split into collided and uncollided parts. The collided part of the particle is forced to react within the current cell, while the uncollided part of the

particle exits the cell without collision. When the track of the uncollided particle portion is continued, it is followed with weight $w_0 e^{-\Sigma_t d}$, where w_0 is the original particle weight and d is the distance traveled between the splitting site and the cell boundary. The collided part of the particle thus reacts with weight $w_0 \left(1 - e^{-\Sigma_t d}\right)$. These resultant weights are chosen to reflect the actual physics of the problem; $e^{-\Sigma_t d}$ is the probability of exiting the cell without collision, and $1 - e^{-\Sigma_t d}$ is the probability of colliding in the cell. One of these two things must happen to the original particle of weight w_0, so we observe that the starting weight is preserved.

Finally, particle sources may be biased with respect to one or more variables. This allows for greater numbers of particles to be produced in more important ranges of each biased variable, with the particles' weights reduced accordingly. In the relevant example of the neutron shielding problem, one may start more particles at high energies and in strategic directions in order to get more particles to contribute to the desired solution. The corresponding weights of the particles are altered to correct the statistical distribution.

2.1.2 Deterministic Methods

In the case of deterministic methods, each of the six independent variables of the steady-state NTE is discretized, relevant boundary conditions are imposed, and the resulting system of linear algebraic equations is iterated over until an acceptable solution has been reached. We limit the discussion here to the discretization of the integro-differential form of the NTE and the finite-volume discrete ordinates method.

These discretizations introduce some errors into the calculations, with the discretization of some variables being more problematic than others. For example, it is functionally straightforward to discretize the energy and spatial variables, while discretizing angular space using the discrete ordinates method is more mathematically intricate and often brings deleterious errors ("ray effects") into problem solutions. Deterministic methods may converge more quickly than Monte Carlo methods, especially in the case of shielding problems, though the solutions are often plagued by the aforementioned inaccuracies.

2.1.2.1 Discretization of the Neutron Transport Equation

Energy Discretization - The Multigroup Approximation

Discretization of the energy variable is known as the "multigroup" approximation; it is relatively straightforward from a mathematical standpoint. Energy is broken up into G groups, where the g^{th} group has an upper bound of energy E_g and a lower bound of energy E_{g+1} as shown in Figure 2.2. The highest energy group has $g = 0$ and the lowest energy group has $g = G - 1$. This convention is used because neutrons are generally born at higher energies (starting in group 0 or 1) and scatter down to lower energies before undergoing an absorption reaction.

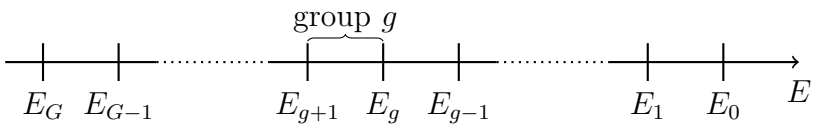

Figure 2.2: Discretized energy grid.

Discretizing the NTE with respect to energy on this grid gives the G multigroup equations

$$\mathbf{\Omega}\cdot\nabla\psi^g(\mathbf{r},\mathbf{\Omega})+\Sigma_t^g(\mathbf{r})\psi^g(\mathbf{r},\mathbf{\Omega})= \sum_{g'=0}^{G-1}\int_{4\pi}\Sigma_s^{g'\to g}(\mathbf{r},\mathbf{\Omega}'\cdot\mathbf{\Omega})\psi^{g'}(\mathbf{r},\mathbf{\Omega}')d\mathbf{\Omega}'+Q^g(\mathbf{r},\mathbf{\Omega}), \quad g=0,1,\ldots,G-1. \tag{2.11}$$

Here it is assumed that, within each energy group, the angular flux may be approximated as the product of some known function of energy $f(E)$ and the group flux $\psi^g(\mathbf{r},\mathbf{\Omega})$ as

$$\psi(\mathbf{r},E,\mathbf{\Omega})\approx f(E)\psi^g(\mathbf{r},\mathbf{\Omega}),\quad E_{g+1}<E\leq E_g\,, \tag{2.12}$$

where $f(E)$ is normalized such that $\int_{E_g+1}^{E_g} f(E)dE=1$. With this, the multigroup cross sections and the group source are similarly defined [1] as

$$\Sigma_t^g(\mathbf{r})=\int_{E_{g+1}}^{E_g}\Sigma_t(\mathbf{r},E)f(E)dE, \tag{2.13}$$

$$\Sigma_s^{g'\to g}(\mathbf{r},\mathbf{\Omega}'\cdot\mathbf{\Omega})=\int_{E_{g+1}}^{E_g}\int_{E_{g'+1}}^{E_{g'}}\Sigma_s(\mathbf{r},E'\to E,\mathbf{\Omega}'\cdot\mathbf{\Omega})f(E')dE'dE, \tag{2.14}$$

$$Q^g(\mathbf{r},\mathbf{\Omega})=\int_{E_{g+1}}^{E_g}Q(\mathbf{r},E,\mathbf{\Omega})dE. \tag{2.15}$$

Spatial Discretization

In the interest of completeness, we will briefly discuss the discretization of space. The LDO equations are inherently three-dimensional [4], so we will restrict the discussion to three-dimensional space with point positions specified by Cartesian coordinates. A general mesh cell is shown in Figure 2.3.

The mesh cell is centered at the i^{th} position along the x-axis, the j^{th} position along the y-axis, and the k^{th} position along the z-axis. Indexing is such that there are I mesh cells with $I+1$ grid points in the x-direction, J mesh cells with $J+1$ grid points in the y-direction, and K mesh cells with $K+1$ grid points in the z-direction. It is assumed that all material properties are constant within a given cell. In order to eventually solve for the scalar flux in a given system, we are interested in solving for the angular flux at the center of each mesh cell, resulting in the $G\times I\times J\times K$ equations shown in Equation 2.16.

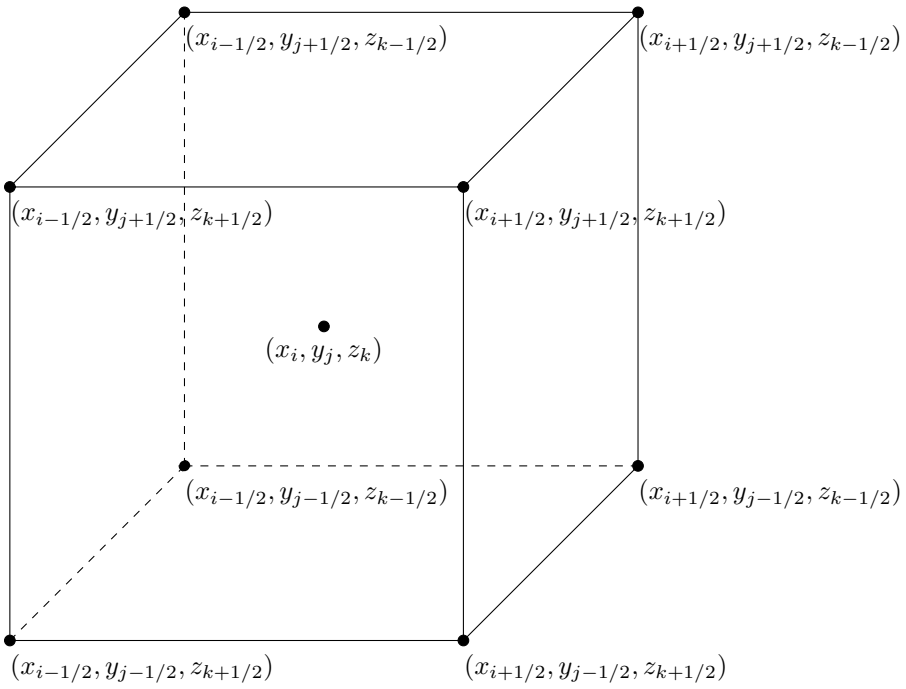

Figure 2.3: General three-dimensional mesh cell [5].

$$\begin{aligned} \boldsymbol{\Omega} \cdot \nabla \psi^g_{i,j,k}(\boldsymbol{\Omega}) + \Sigma^g_{t,i,j,k} \psi^g_{i,j,k}(\boldsymbol{\Omega}) = & \qquad g = 0, 1, \ldots, G-1, \\ \sum_{g'=0}^{G-1} \int_{4\pi} \Sigma^{g' \to g}_{s,i,j,k}(\boldsymbol{\Omega}' \cdot \boldsymbol{\Omega}) \psi^{g'}_{i,j,k}(\boldsymbol{\Omega}') d\boldsymbol{\Omega}' + Q^g_{i,j,k}(\boldsymbol{\Omega}), & \qquad \begin{aligned} i &= 1, 2, \ldots, I, \\ j &= 1, 2, \ldots, J, \\ k &= 1, 2, \ldots, K. \end{aligned} \end{aligned} \tag{2.16}$$

To solve for these cell-centered flux quantities in practice, auxiliary equations are introduced. As these are specific to the spatial discretization employed in a given solution and do not differ between the classical discrete ordinates equations and the LDO formulation, we refer the reader to Reference [6] for more detail on spatial differencing and solution methods.

Angular Discretization - Discrete Ordinates

The last part of phase space to discretize in the time-independent NTE is angle. The discrete ordinates method is the most common angular discretization method incorporated into general-purpose neutron transport codes [1]. It is a collocation method that requires the solution of the NTE to be exact at a distinct number of angles $\boldsymbol{\Omega}_n$:

$$\begin{aligned}
&\boldsymbol{\Omega}_n \cdot \nabla \psi^{g,n}_{i,j,k} + \Sigma^{g}_{t,i,j,k}\psi^{g,n}_{i,j,k} = && g = 0, 1, \ldots, G-1, \\
&\quad \sum_{g'=0}^{G-1}\sum_{\ell=0}^{P} \Sigma^{g'\to g}_{s,\ell,i,j,k}\left[Y^{e}_{\ell 0}(\boldsymbol{\Omega}_n)\phi^{g'}_{\ell 0} + \sum_{m=1}^{\ell}\left(Y^{e}_{\ell m}(\boldsymbol{\Omega}_n)\phi^{g'}_{\ell m} \right.\right. && i = 1, 2, \ldots, I, \\
&\qquad \left.\left. + Y^{o}_{\ell m}(\boldsymbol{\Omega}_n)\vartheta^{g'}_{\ell m} \right)\right] + Q^{g,n}_{i,j,k}, && j = 1, 2, \ldots, J, \\
& && k = 1, 2, \ldots, K, \\
& && n = 1, 2, \ldots, N.
\end{aligned} \tag{2.17}$$

Here, $\psi^n \equiv \psi(\boldsymbol{\Omega}_n)$ and the angles are integrated by a quadrature rule such that their corresponding weights w_n sum to 4π. Weights and ordinates ("quadrature sets") are chosen in such a way as to provide good approximations to angular integrals used to evaluate scalar flux [1, 5]. The upper limit of summation for the scattering term spherical harmonic expansion, denoted as P in Equation 2.17, is known as the "$\mathrm{P_N}$ order". The scattering cross section coefficient values $\Sigma^{g'\to g}_{s,\ell,i,j,k}$ come from data libraries based on experimental measurements.

The scattering source is expanded in terms of spherical harmonics:

$$\phi^{g}_{\ell,i,j,k} = \sum_{n=1}^{N} Y^{e}_{\ell m}(\boldsymbol{\Omega}_n) w_n \psi^{g,n}_{i,j,k} \quad \text{and} \quad \vartheta^{g}_{\ell,i,j,k} = \sum_{n=1}^{N} Y^{o}_{\ell m}(\boldsymbol{\Omega}_n) w_n \psi^{g,n}_{i,j,k}, \tag{2.18}$$

where ϕ and ϑ are referred to as the "flux moments". Here, $Y^{e}_{\ell m}(\boldsymbol{\Omega}_n)$ and $Y^{o}_{\ell m}(\boldsymbol{\Omega}_n)$ are the "even" and "odd" real components of the spherical harmonic functions, defined as [5]

$$Y^{e}_{\ell m}(\boldsymbol{\Omega}_n) = (-1)^m \sqrt{(2-\delta_{m0})\frac{2\ell+1}{4\pi}\frac{(\ell-m)!}{(\ell+m)!}} P_{\ell m}(\cos\theta)\cos(m\varphi), \tag{2.19}$$

$$Y^{o}_{\ell m}(\boldsymbol{\Omega}_n) = (-1)^m \sqrt{(2-\delta_{m0})\frac{2\ell+1}{4\pi}\frac{(\ell-m)!}{(\ell+m)!}} P_{\ell m}(\cos\theta)\sin(m\varphi). \tag{2.20}$$

In Equations 2.19 and 2.20, $P_{\ell m}(\cos\theta)$ is the associated Legendre polynomial and (θ, φ) are the components of $\boldsymbol{\Omega}$ as shown in Figure 2.4 and Equations 2.21a – 2.22. It is assumed that the double differential scattering cross section depends only on the dot product of the incoming and outgoing angles of the particle undergoing scattering.

To summarize Equations 2.17 – 2.20, we note that the double differential scattering cross section is expanded into the real components of the spherical harmonic functions, which can be represented with Legendre polynomials; these are then multiplied with the angular flux moments expanded into spherical harmonic functions.

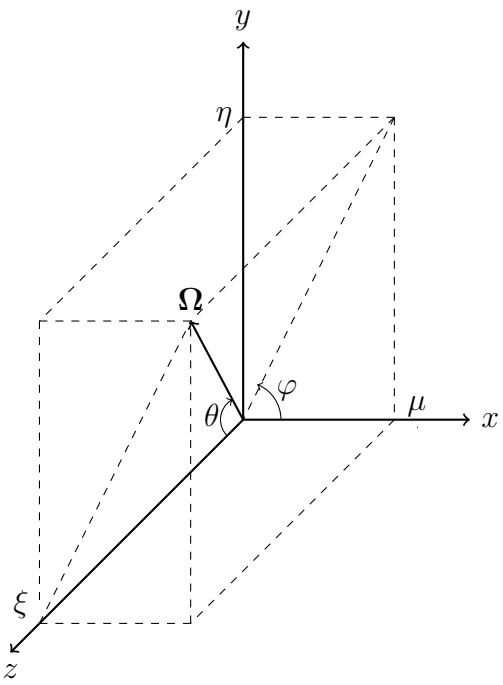

$$\xi = \cos\theta \tag{2.21a}$$

$$\mu = \sqrt{1-\xi^2}\cos\varphi \tag{2.21b}$$

$$\eta = \sqrt{1-\xi^2}\sin\varphi \tag{2.21c}$$

$$\mu^2 + \eta^2 + \xi^2 = 1 \tag{2.22}$$

Figure 2.4: Angular coordinate system [5].

Commonly-used quadrature sets include level-symmetric, Gauss- Legendre product, quadruple range (QR) product, and linear-discontinuous finite element (LDFE). The various quadrature set types have different properties with each being better for certain classes of problems. For example, relatively coarse (sixteen angles per octant) QR product quadratures are generally sufficient for generating variance reduction parameters for neutron transport problems, but more finely resolved quadrature sets are recommended for photon transport problems [7]. Level-symmetric quadrature sets are widely applied for general applications [1] but tend to exhibit far more ray effects than QR product quadratures [7]. In the following subsection, we will discuss ray effects in greater detail.

2.1.2.2 Ray Effects

Ray effects are unphysical computational anomalies in the scalar flux solution that arise from the discrete ordinates formulation. Because the NTE is only evaluated at a finite number of discrete angles, the number of directions in which particles may stream is restricted. As a consequence of this, contributions to the scalar flux from uncollided particles are limited to those from the discrete angles along which particle sources are "visible" [8]. A demonstrative example of ray effects is shown in Figure 2.5. The plot shows results from the PARTISN [9] code using a triangular $P_n - T_n$ quadrature with 48 points and a scattering ratio of $c = 0.25$ [4]. Although the point source emits neutrons isotropically, the scalar flux calculated at a given radius out from the source sees contributions only from the discrete angles along which

particles may stream. That is, the flux at a given distance from the point source is actually equal in all directions and so the figure should appear to be a sphere, but the discrete angles restrict streaming pathways to the rays shown in the image.

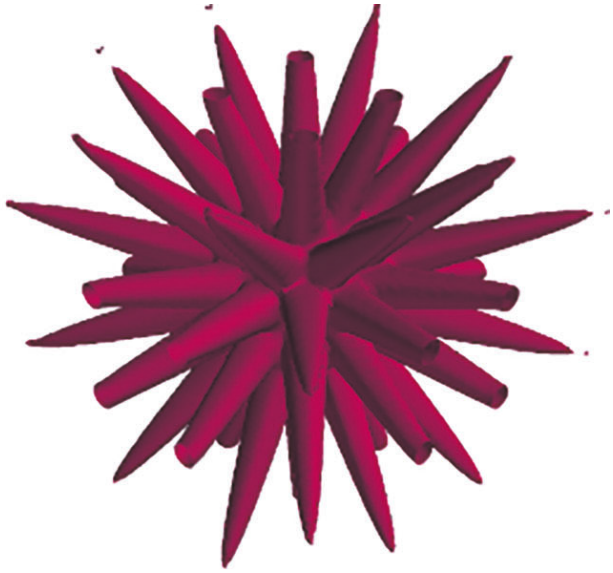

Figure 2.5: Isosurface plot of scalar flux from a point source [4].

The severity of ray effects in a given simulation depends on the properties of the sources. The largest consequences tend to occur in scenarios with localized sources and relatively minimal scattering. When using the discrete ordinates approximation in a purely absorbing medium, regardless of the accuracy of the angular flux calculations and the number of discrete angles used, it is always possible to get far enough away from a localized source such that a poor value of the scalar flux is obtained at that point [8]. In a scattering medium with localized sources, angular flux values are incorrect because they depend on integrals that are poorly approximated by the quadrature formulation. In contrast to this, neutrons exiting scattering reactions are generally less localized and consequently tend to mitigate ray effects. As we will see later in the chapter, one key point of interest in using the LDO equations as part of a hybrid method calculation is that the LDO equations mitigate ray effects when higher-order quadrature sets are used [4].

2.1.3 Hybrid Methods

Hybrid methods aim to combine the previously described Monte Carlo methods and deterministic methods in such a way as to perform calculations that result in statistically meaningful results within a tractable period of computation time. Generally, these hybrid methods are implemented such that the solution(s) from a deterministic code are used to inform a Monte Carlo code. When this is done well, the Monte Carlo code converges more quickly than without the information from the deterministic solution(s).

Specifically, an adjoint and/or forward flux solution generated by a deterministic transport solver is used to make a weight window map for a Monte Carlo run. As was noted earlier, weight windows are most effective when specified well and when used in conjunction with other variance reduction techniques. Because developing effective weight window maps can be labor-intensive and require a user to have significant *a priori* knowledge about the problem being solved, automated hybrid methods have been developed to couple deterministic solutions to Monte Carlo transport calculations.

2.2 Previous Work

Substantial effort has been placed into the development and automated execution of hybrid methods. This section will discuss previous work in this field with a particular emphasis on the present state of hybrid methods as well as hybrid methods that incorporate neutron direction of travel.

Here we begin by describing the CADIS (consistent adjoint driven importance sampling) and FW-CADIS (forward-weighted consistent adjoint driven importance sampling) methods, which are the current state of the art of Monte Carlo variance reduction parameter generation. These are introduced first because, as will be described in more detail later, this work employs solutions of the LDO equations in combination with the CADIS and FW-CADIS methods via the ADVANTG software. Following this, we present a discussion of selected work in angle-informed hybrid methods, focusing on variants of CADIS and FW-CADIS.

2.2.1 CADIS and FW-CADIS

2.2.1.1 CADIS

The CADIS method was introduced by Wagner and Haghighat in 1997 to automate Monte Carlo variance reduction parameter generation [10]. CADIS is based on the source biasing and weight window techniques described above, does not depend heavily on user experience, and was implemented as described in Reference [10] in the MCNP [2] code. Most importantly, the CADIS method produces source biasing parameters and weight window target values such that particles are born with the target weights. Since CADIS is used heavily in this work, it is pertinent to describe the theory behind the method.

The goal of most Monte Carlo neutron transport problems is to calculate some response (scalar flux, dose, etc.) at some location in phase-space. This can be posed as solving the following integral equation:

$$R = \int_P \psi(P)\sigma_d(P)dP, \tag{2.23}$$

where R is the response of interest, ψ is the neutron angular flux, and σ_d is some objective function in the phase-space $(\mathbf{r}, E, \mathbf{\Omega}) \in P$. We now introduce the adjoint identity

$$\langle \psi^\dagger, H\psi \rangle = \langle \psi, H^\dagger \psi^\dagger \rangle \tag{2.24}$$

where H is the transport operator and the dagger superscript indicates an adjoint quantity. Using Equation 2.24 and some algebraic manipulations, it can be shown that

$$R = \int_P \psi^\dagger(P) q(P) dP, \tag{2.25}$$

where $\psi^\dagger$ and q are the adjoint neutron angular flux function and the particle source density, respectively. For a given problem with a vacuum boundary condition, Equations 2.23 and 2.25 are equivalent expressions for R. The adjoint neutron angular flux function $\psi^\dagger$ has physical meaning as the expected contribution to the response R from a particle in phase-space P. In other words, the adjoint flux function is significant because it represents the importance of those source particles to the response of interest.

To calculate the response with the Monte Carlo method, the independent variables are sampled from the probability density function (PDF) $q(P)$. However, this may not be the best PDF from which to sample, so an alternative PDF $\hat{q}(P)$ can be introduced into the integral:

$$R = \int_P \left[\frac{\psi^\dagger(P) q(P)}{\hat{q}(P)} \right] \hat{q}(P) dP, \tag{2.26}$$

where $\hat{q}(P) \geq 0$ and the integral of $\hat{q}(P)$ over P is normalized to unity. Then, the alternative PDF $\hat{q}(P)$ that will minimize the variance of the response is given by

$$\hat{q}(P) = \frac{\psi^\dagger(P) q(P)}{\int_P \psi^\dagger(P) q(P) dP}. \tag{2.27}$$

Looking at Equation 2.27, we see that the numerator is the response from phase-space P and the denominator is the total response R. Thus, this definition of $\hat{q}(P)$ is a measure of the contribution from phase-space P to the response. It is useful to bias the sampling of source particles by this ratio of their contribution to the detector response.

Because the source variables are sampled from this new biased PDF, the statistical weight of the source particles must be corrected such that

$$w(P)\hat{q}(P) = w_0 q(P), \tag{2.28}$$

where w_0 is the unbiased particle starting weight and is set equal to 1. Substituting Equation 2.27 into Equation 2.28 and solving for $w(P)$ gives the following expression for the statistical weight of the particles:

$$w(P) = \frac{\int_P \psi^\dagger(P) q(P) dP}{\psi^\dagger(P)} = \frac{R}{\psi^\dagger(P)}. \tag{2.29}$$

Equation 2.29 demonstrates an inverse relationship between this adjoint (importance) function and the statistical particle weight.

Now, let us consider the transport process in this context. The integral transport equation for particle density in the phase-space P is given by

$$\psi(P) = \int K(P' \to P)\psi(P')dP' + q(P) \tag{2.30}$$

where $K(P' \to P)$ is the expected number of particles entering dP about P from an event in P'. Given the preceding discussion, we would like to transform Equation 2.30 to be in terms of the biased source distribution $\hat{q}(P)$. Defining

$$\hat{\psi}(P) = \frac{\psi(P)\psi^\dagger(P)}{\int \psi^\dagger(P)q(P)dP}, \tag{2.31}$$

we can write Equation 2.30 in terms of $\hat{q}(P)$ as

$$\hat{\psi}(P) = \frac{\psi^\dagger(P)}{\int \psi^\dagger(P)q(P)dP} \int K(P' \to P)\psi(P')dP' + \hat{q}(P). \tag{2.32}$$

Equation 2.32 can also be written as

$$\hat{\psi}(P) = \int K(P' \to P)\hat{\psi}(P') \left[\frac{\psi^\dagger(P)}{\psi^\dagger(P')}\right] dP' + \hat{q}(P)\,, \tag{2.33}$$

which allows us to define

$$\hat{K}(P' \to P) = K(P' \to P) \left[\frac{\psi^\dagger(P)}{\psi^\dagger(P')}\right] \tag{2.34}$$

and finally write

$$\hat{\psi}(P) = \int \hat{K}(P' \to P)\hat{\psi}(P')dP' + \hat{q}(P). \tag{2.35}$$

Because $K(P' \to P)$ is unknown, we simulate neutron transport in the usual unbiased way and change the number of particles emerging in P from an event in P' by the ratio of importances $\psi^\dagger(P)/\psi^\dagger(P')$. When this ratio is above one, splitting occurs, and rouletting occurs when the ratio is less than one. The statistical weights of the particles resulting from splitting and/or rouletting are then corrected such that

$$w(P)K(P' \to P) \left[\frac{\psi^\dagger(P)}{\psi^\dagger(P')}\right] = w(P')K(P' \to P) \tag{2.36}$$

or

$$w(P) = w(P') \left[\frac{\psi^\dagger(P)}{\psi^\dagger(P')}\right]. \tag{2.37}$$

With this, reduced variance can be achieved when all source and transport sampling is proportional to its importance. The source particles' energy and position are sampled from the biased source distribution

$$\hat{q}(\mathbf{r}, E) = \frac{\phi^{\dagger}(\mathbf{r}, E) q(\mathbf{r}, E)}{\int_V \int_E \phi^{\dagger}(\mathbf{r}, E) q(\mathbf{r}, E) dE \; d\mathbf{r}} = \frac{\phi^{\dagger}(\mathbf{r}, E) q(\mathbf{r}, E)}{R}. \tag{2.38}$$

Here, the physical meaning of the numerator is the detector response from space-energy element $(d\mathbf{r}, dE)$ and the denominator is the total detector response R. As in the preceding derivation, this ratio is a measure of the particles' relative contribution to the detector response.

To bias particles undergoing the transport process, the weight window technique is applied. Weight window lower bounds w_ℓ must be calculated such that the statistical weights defined in Equation 2.29 fall at the center of the weight window intervals. The width of a given interval is denoted by $c_u = w_u / w_\ell$, the ratio of upper and lower weight window values. The weight window lower bounds are then given by

$$w_\ell(\mathbf{r}, E) = \frac{w}{\left(\frac{c_u+1}{2}\right)} = \frac{R}{\phi^{\dagger}(\mathbf{r}, E)} \frac{1}{\left(\frac{c_u+1}{2}\right)}. \tag{2.39}$$

Using this definition, the weight window technique then performs particle splitting and/or rouletting consistent with the statistical weight given in Equation 2.37.

The key result of the foregoing discussion is that the statistical weights of the source particles are within the bounds of the weight windows. In other words, the source-biasing parameters and the weight window target values are consistent. This circumvents the potential of particles being immediately split or rouletted upon birth and avoids the resultant degradation in computational efficiency. We refer the reader to Reference [10] for a complete discussion of results and analysis of the initial implementation of the CADIS method.

Note that Equations 2.38 and 2.39 use the scalar adjoint flux rather than the angular flux. This is consistent with the original implementation of the CADIS method in MCNP as well as the implementation of the method in ADVANTG; the scalar adjoint neutron flux function is used in both tools [10, 7]. Historically, this was done to reduce the memory required for the deterministic calculation as well as the weight window map. Additionally, the angular adjoint flux resulting from an S_N calculation was not considered to be sufficiently accurate due to the limited number of discrete angles used for the calculation. Further, people have generally not developed weight windows that are a function of angle.

The CADIS method is very effective for automated optimization of localized detectors but falls short of efficiently optimizing distributed responses. FW-CADIS, discussed in the next section, was developed to address this issue.

2.2.1.2 FW-CADIS

FW-CADIS, introduced by Wagner, Blakeman, and Peplow in 2009, is a variation on the CADIS method to increase the efficiency of Monte Carlo calculations of distributions and

responses at multiple localized detectors [11].

For this global variance reduction method, a response with uniformly-low statistical uncertainty across all phase-space is desired. One way to target this for a given Monte Carlo simulation is to uniformly distribute the particles throughout the system. Though this is not a physical response, it is a proxy for the goal of obtaining uniform uncertainty. It also indicates the possibility of developing an adjoint importance function that represents the importance of particles to achieving the goal of uniform particle distribution.

With this new problem formulation, the problem of calculating particle density is cast into the response formulation:

$$R = \int_{4\pi} \int_V \int_E \psi(\mathbf{r}, E, \mathbf{\Omega}) f(\mathbf{r}, E, \mathbf{\Omega}) dE \; dV \; d\mathbf{\Omega}, \tag{2.40}$$

where $f(\mathbf{r}, E, \mathbf{\Omega})$ is some function that converts angular neutron flux to Monte Carlo particle density. Recall that the angular neutron flux can be defined as the product of the physical particle density n and velocity v:

$$\psi(\mathbf{r}, E, \mathbf{\Omega}) = n(\mathbf{r}, E, \mathbf{\Omega}) v(\mathbf{r}, E, \mathbf{\Omega}) \tag{2.41}$$

and the physical particle density is related to the Monte Carlo particle density m and the average particle weight $\bar{w}$ by

$$n(\mathbf{r}, E, \mathbf{\Omega}) = \bar{w}(\mathbf{r}, E, \mathbf{\Omega}) m(\mathbf{r}, E, \mathbf{\Omega}). \tag{2.42}$$

Using Equations 2.41 and 2.42, the Monte Carlo particle density can be estimated by

$$m(\mathbf{r}, E, \mathbf{\Omega}) = \frac{n(\mathbf{r}, E, \mathbf{\Omega})}{\bar{w}(\mathbf{r}, E, \mathbf{\Omega})} = \frac{\psi(\mathbf{r}, E, \mathbf{\Omega})}{\bar{w}(\mathbf{r}, E, \mathbf{\Omega}) v(\mathbf{r}, E, \mathbf{\Omega})} \tag{2.43}$$

and the total Monte Carlo density can be estimated by

$$R = \int_{4\pi} \int_V \int_E \psi(\mathbf{r}, E, \mathbf{\Omega}) \left[\frac{1}{\bar{w}(\mathbf{r}, E, \mathbf{\Omega}) v(\mathbf{r}, E, \mathbf{\Omega})} \right] dE \; dV \; d\mathbf{\Omega}. \tag{2.44}$$

If the average particle weight is set proportional to the physical particle density, then the Monte Carlo particle density should be approximately uniform in phase-space. Substituting Equation 2.41 into Equation 2.44 gives

$$R = \int_{4\pi} \int_V \int_E \psi(\mathbf{r}, E, \mathbf{\Omega}) \left[\frac{1}{\psi(\mathbf{r}, E, \mathbf{\Omega})} \right] dE \; dV \; d\mathbf{\Omega}. \tag{2.45}$$

By then defining the adjoint source as the bracketed term in the above equation,

$$q^\dagger(\mathbf{r}, E, \mathbf{\Omega}) = \frac{1}{\psi(\mathbf{r}, E, \mathbf{\Omega})}, \tag{2.46}$$

we can calculate an adjoint importance function that represents the importance of particles to achieving the desired objective of uniformly distributed Monte Carlo particles. This

should, in turn, correspond to approximately uniform statistical uncertainties. The method physically corresponds to weighting the adjoint source with the inverse of the forward flux; the adjoint source will be high where the forward flux is low and the adjoint source will be low where the forward flux is high. With this method, after the adjoint has been determined, the standard CADIS procedures are used to calculate consistent source biasing parameters and weight windows.

When considering implementation and use, it should be noted that, while the original CADIS method requires only one deterministic calculation, the FW-CADIS method requires two (one forward and one adjoint) deterministic calculations. Additionally, like the original CADIS method, FW-CADIS is general and could be applied to all independent variables of a problem, but the implementation has been limited to space and energy.

2.2.2 Directional CADIS

Noting the marked performance of the CADIS and FW-CADIS methods, their limited implementation in only space and energy, and the importance of particle direction, Peplow introduced directional CADIS in 2012 [12]. Two versions of directional CADIS were explored: one method that biases the source in space and energy while preserving the original angular distribution of the particles, and one method that biases the source in space, energy, and angle. Both new methods were tested against standard CADIS for seven example problems, with the Monte Carlo FOM compared among the methods for each problem.

Peplow notes that in many applications involving directionally dependent source distributions, the directional dependence is azimuthally symmetric about a given reference direction $\hat{\mathbf{d}}$. With this, the angular distribution of the particles $q_i(\mathbf{\Omega})$ can be expressed as the product of the uniform azimuthal distribution and a polar distribution about reference $\hat{\mathbf{d}}_i$. The angular particle distribution may then be written as $\frac{1}{2\pi} q_i(\mathbf{\Omega} \cdot \hat{\mathbf{d}}_i)$. Peplow also notes that the geometric size of these directional sources tends to be small enough to allow each source distribution to be expressed as the product of two separable distributions: $q_i(\mathbf{r}, E, \mathbf{\Omega}) \approx q_i(\mathbf{r}, E) q_i(\mathbf{\Omega})$.

The implementation of directional CADIS explored in this work was intended to appropriately incorporate the importance of a particle traveling in a given direction while also serving as a relatively simple modification of the standard CADIS method that is less involved than a full treatment of space, energy, and angle. It starts with the approximation that the angular component of the adjoint flux $\psi^\dagger(\mathbf{r}, E, \mathbf{\Omega})$ is separable and symmetric about the average adjoint current direction $\hat{\mathbf{n}}(\mathbf{r}, E)$ such that

$$\psi^\dagger(\mathbf{r}, E, \mathbf{\Omega}) \approx \phi^\dagger(\mathbf{r}, E) \frac{1}{2\pi} f(\mathbf{\Omega} \cdot \hat{\mathbf{n}}). \tag{2.47}$$

From this, it is proposed that weight window targets can be developed that are inversely proportional to the approximation of the adjoint angular flux:

$$\bar{w}(\mathbf{r}, E, \mathbf{\Omega}) = \frac{2\pi k}{\phi^{\dagger}(\mathbf{r}, E) f(\mathbf{\Omega} \cdot \hat{\mathbf{n}})} \tag{2.48}$$

where k is a constant of proportionality that is adjusted to make the importance map consistent with the biased source(s). The implementation of the following methods uses standard CADIS routines to compute the response per unit source R, the weight window target values $\bar{w}(\mathbf{r}, E)$, and the biased source $\hat{q}(\mathbf{r}, E)$ using only the adjoint scalar flux. The quantities are then modified to include directional information.

2.2.2.1 Without Directional Source Biasing

Peplow asserts that the biased source $\hat{q}(\mathbf{r}, E, \mathbf{\Omega})$ should be proportional to both the true particle source distribution and the space-energy component of the scalar adjoint flux:

$$\hat{q}(\mathbf{r}, E, \mathbf{\Omega}) = \frac{1}{R} \left[q(\mathbf{r}, E) \frac{1}{2\pi} q(\mathbf{\Omega} \cdot \hat{\mathbf{d}}) \right] \phi^{\dagger}(\mathbf{r}, E), \tag{2.49}$$

where the constant of proportionality R is determined by forcing $\hat{q}(\mathbf{r}, E, \mathbf{\Omega})$ to be a PDF. Since the scalar adjoint flux is used here, the directional distribution of the biased source is identical to that of the true source. Detailed in Reference [12], the constant of proportionality R is found to be equal to the response per unit source from the traditional space-energy CADIS treatment. Thus, the biased source can be expressed as

$$\hat{q}(\mathbf{r}, E, \mathbf{\Omega}) = \hat{q}(\mathbf{r}, E) \frac{1}{2\pi} q(\mathbf{\Omega} \cdot \hat{\mathbf{d}}). \tag{2.50}$$

The birth weight of a particle sampled from this distribution is independent of direction and the proportionality constant k for the target weight windows should be chosen such that the weight window targets match the birth weight of the source particles. This cannot be done generally because the particle birth weight is independent of direction, but it can be done for a single point in phase space $(\mathbf{r}_0, E_0, \mathbf{\Omega}_0)$ of the source such that

$$k = \frac{R}{2\pi} f\left(\mathbf{\Omega}_0 \cdot \hat{\mathbf{n}}(\mathbf{r}_0, E_0)\right), \tag{2.51}$$

where the average adjoint current direction $\hat{\mathbf{n}}(\mathbf{r}_0, E_0)$ is evaluated at the source location and energy and

$$\bar{w}(\mathbf{r}, E, \mathbf{\Omega}) = \bar{w}(\mathbf{r}, E) \frac{f\left(\mathbf{\Omega}_0 \cdot \hat{\mathbf{n}}(\mathbf{r}_0, E_0)\right)}{f(\mathbf{\Omega} \cdot \hat{\mathbf{n}})}. \tag{2.52}$$

Because the biased source and the weight window targets will match only at the specified direction of interest $\mathbf{\Omega}_0$ at one specific position and energy, the point $(\mathbf{r}_0, E_0, \mathbf{\Omega}_0)$ should be chosen carefully to represent the source accurately and to minimize rouletting and/or splitting of particles just after birth.

It should be noted that this approach is exact for cases where no directional biasing could be applied, e.g. monodirectional beam sources. Although the above discussion considers only one particle source, this directional CADIS method may be extended to multiple sources, as explained in detail in Reference [12].

2.2.2.2 With Directional Source Biasing

In this method, it is asserted that the biased source should be proportional to both the true particle source distribution and the approximation of the angular adjoint flux:

$$\hat{q}(\mathbf{r}, E, \mathbf{\Omega}) = \frac{1}{cR}\left[q(\mathbf{r}, E)\frac{1}{2\pi}q(\mathbf{\Omega}\cdot\hat{\mathbf{d}}_i)\right]\left[\phi^{\dagger}(\mathbf{r}, E)\frac{1}{2\pi}f(\mathbf{\Omega}\cdot\hat{\mathbf{n}}_0)\right], \tag{2.53}$$

where the constant cR is used to make $\hat{q}$ a PDF. Because the vector $\hat{\mathbf{n}}_0$ is fixed over the source, the biased source is separable into $\hat{q}(\mathbf{r}, E, \mathbf{\Omega}) = \hat{q}(\mathbf{r}, E)\hat{q}(\mathbf{\Omega})$ where $\hat{q}(\mathbf{\Omega})$ can be further separated into the product of its azimuthal and polar distributions:

$$\hat{q}(\mathbf{r}, E, \mathbf{\Omega}) = \left[\frac{1}{R}q(\mathbf{r}, E)\phi^{\dagger}(\mathbf{r}, E)\right]\left[\frac{1}{c}\frac{1}{4\pi^2}q(\mathbf{\Omega}\cdot\hat{\mathbf{d}})f(\mathbf{\Omega}\cdot\hat{n}_0)\right]. \tag{2.54}$$

Both distributions $\hat{q}(\mathbf{r}, E)$ and $\hat{q}(\mathbf{\Omega})$ are independent and each should be a PDF. For the space-energy distribution, the standard definition of R still applies. For the angular distribution, the constant c is found to be

$$c = \int \frac{1}{4\pi^2}q(\mathbf{\Omega}\cdot\hat{\mathbf{d}})f(\mathbf{\Omega}\cdot\hat{\mathbf{n}}_0)d\mathbf{\Omega}, \tag{2.55}$$

which may be evaluated using numerical integration. It should be noted that if either the original source directional distribution $q(\mathbf{\Omega})$ or the adjoint angular flux distribution at the source is isotropic, then c reduces to a value of $\frac{1}{4\pi}$.

Source particles sampled from the biased distribution are born with a starting weight of

$$\bar{w}(\mathbf{r}, E, \mathbf{\Omega}) = \frac{R}{\phi^{\dagger}(\mathbf{r}, E)}\frac{2\pi c}{f(\mathbf{\Omega}\cdot\hat{\mathbf{n}}_0)} = \bar{w}(\mathbf{r}, E)\frac{2\pi c}{f(\mathbf{\Omega}\cdot\hat{\mathbf{n}}_0)}, \tag{2.56}$$

where the constant k has been found to be equal to cR. As with the previously described method, the user selects one point $(\mathbf{r}_0, E_0, \mathbf{\Omega}_0)$ that is representative of the entire source, where the biased source will match the target weight windows. This method can also be extended to incorporate multiple sources.

2.2.2.3 Results

Sample problems of applications of interest were examined and compared between standard CADIS and directional CADIS. For most of these problems, directional CADIS outperformed standard CADIS, increasing the Monte Carlo FOM by a factor of around 2. Notable cases in which directional CADIS performed more poorly than standard CADIS are a neutron

porosity tool problem and a gamma-ray litho-density tool problem with the detector far away from the source. It should also be noted that, for a spherical boat test problem with a source far away from the boat, both standard CADIS and directional CADIS performed more poorly than an analog Monte Carlo calculation. For full details on the test results, see Reference [12]. In the conclusions of the report, Peplow notes that "it is difficult to know *a priori* which problems would benefit from the space/energy/angular treatments presented in this work more than from just using the standard space/energy CADIS."

2.2.3 CADIS-Ω

One of the most recent developments in the area of angle-informed hybrid methods is CADIS-Ω, introduced by Munk et al. in 2016 [13]. This method calculates an alternate form of the adjoint scalar flux quantity that is then used in the CADIS and FW-CADIS methods for generation of variance reduction parameters for local and global response functions, respectively.

The alternative form of the adjoint scalar flux used in CADIS-Ω is defined as

$$\phi_{\Omega}^{\dagger}(\mathbf{r}, E) = \frac{\int_{4\pi} \psi(\mathbf{r}, E, \mathbf{\Omega})\psi^{\dagger}(\mathbf{r}, E, \mathbf{\Omega})d\mathbf{\Omega}}{\int_{4\pi} \psi(\mathbf{r}, E, \mathbf{\Omega})d\mathbf{\Omega}}. \tag{2.57}$$

Here, the product $\psi(\mathbf{r}, E, \mathbf{\Omega})\psi^{\dagger}(\mathbf{r}, E, \mathbf{\Omega})$ is known as the "contributon flux"; contributons can be conceptualized as pseudo-particles that carry "response" from a particle source to a detector. The contributon flux incorporates information from both the forward particle flux as well as the adjoint particle flux. It signifies the importance of a particle born from a forward source moving towards an adjoint source. That is, when the contributon flux is used to generate an importance map, high importance will be assigned to particles that are generated at the forward source and are likely to generate a response in the detector (the adjoint source).

The CADIS-Ω method was implemented in the ADVANTG framework, with numerical experiments performed testing variance reduction for problems run in MCNP5. Several characterization problems with spatially-induced anisotropies were tested to evaluate the new method when used with CADIS and FW-CADIS. Here we will summarize the problems tested and the results; a full discussion can be found in Reference [14]. Munk identified three categories of processes that affect particle flux anisotropy: strongly directional particle sources, strong differences between material properties, and algorithmic limitations that result in ray effects.

Having grouped these processes, Munk tested a set of characterization problems, each of which have different combinations of the above anisotropy-inducing mechanisms. Munk also developed a set of metrics by which the anisotropy of the flux may be quantified over the various problems. Similar to the conclusions drawn by Peplow, Munk found that it was difficult to predict for which problems CADIS-Ω should outperform CADIS. When considering a parametric study of deterministic variables likely to affect angular flux (varying

quadrature set order and P_N order) in a characteristic problem composed of a steel beam embedded in concrete, CADIS-Ω achieved higher FOM values than standard CADIS for all quadrature and P_N orders at high energies. Similarly, for a simple labyrinth geometry of an air maze through a concrete block, CADIS-Ω achieved lower relative errors than did standard CADIS in the epithermal and fast neutron energy groups.

2.2.4 Other Notable Work

Here we will briefly summarize other notable works in the area of angle-informed hybrid methods. We first introduce AVATAR, then discuss two following methods that built off of the work.

2.2.4.1 AVATAR

AVATAR (Automatic Variance And Time of Analysis Reduction) was developed at Los Alamos National Laboratory by Van Riper et al. in the 1990s to eliminate the need for user-generated weight windows [15]. The package may be thought of as a predecessor to the various CADIS methods, as it constructs three-dimensional energy- and angle-dependent weight windows for an MCNP run from an adjoint calculation using the THREEDANT [16] deterministic code.

The scalar adjoint fluxes resulting from THREEDANT are inverted by AVATAR to get the lower weight window boundary in each mesh element of the problem. The weight windows are then normalized such that source particles are born with weights inside of the weight window. If angle-dependent weight windows are desired, the angular adjoint flux is approximated using information theory [15]; the full angular adjoint flux was deemed to require an inordinate amount of storage at the time of development.

AVATAR's weight window mesh is independent of the Monte Carlo cells, so weight windows are applied at absolute particle positions rather than when particles pass between weight window meshes. To protect against significant variance increases in particle weight (and tally) due to large sampling distance, weight windows are applied at a minimum of once per mean free path traveled by a particle.

AVATAR was tested on a model of a three-detector oil well logging tool consisting of a gamma-ray source and three gadolinium detectors. The system was intended to represent deep-penetration problems, as a small fraction of the gamma rays emitted from the source actually reach the detectors. The detector nearest the gamma-ray source has a collimator attached, adding an angular dependence to the tool modeled.

Results from AVATAR were compared against MCNP's weight window generator (WWG). For the three-detector problem described above, AVATAR's angle-dependent weight windows delivered the highest FOM for the detector nearest the source as well as the "middle" detector. The MCNP WWG delivered the highest FOM for the detector furthest from the source, but it should be noted that the MCNP geometry was hand-tuned for the WWG cases. When

considering only a single detector, the AVATAR angle-dependent weight windows outperformed the WWG for a detector near the source as well as far from the source.

2.2.4.2 Cooper and Larsen's Weight Windows

Cooper and Larsen developed a method similar to FW-CADIS that uses weight windows to distribute Monte Carlo particles uniformly throughout the system for the purpose of efficiently solving global particle transport problems [17]. Rather than using an adjoint deterministic solution for generation of weight windows, a forward solution is used. The method presented employs solution of the forward quasi-diffusion equation, a modified diffusion equation that contains multiplicative correction terms known as "Eddington factors".

The authors argue that a forward solution is more appropriate than an adjoint solution in the context of automated weight window generation for Monte Carlo variance reduction. This is supported by showing that if the center of the weight window in each cell is chosen to be proportional to the density of the physical particles in the cell, then the density of Monte Carlo particles throughout the system will be approximately constant.

Cooper and Larsen construct "isotropic" weight windows as well as angle-dependent weight windows, following the AVATAR method to formulate the latter. The authors note that a uniform particle distribution in angle is not always optimal with respect to computational efficiency, especially when considering problems with significant streaming. It is the case that the angle-dependent weight windows developed in this work actually have the potential to reduce the FOM due to excessive Monte Carlo particle splitting in nonstreaming regions. To mitigate this by decreasing the amount of splitting incurred, the weight window experienced by particles traveling in directions opposite to the preferred direction is raised. This preserves the scalar flux, but not the current [17].

Results are presented for two two-dimensional problems. In both problems, weight windows were updated twice – once after one-third of the histories had completed and again after two-thirds of the particle histories had finished. The weight window parameters were chosen to ensure a stable quasi-diffusion solution. The two problems were chosen to rigorously test the global Monte Carlo method; the problems are optically thick with scattering ratios sufficiently low such that the scalar flux decreases by several orders of magnitude far away from the particle source. To observe the performance of the method on problems with significant angular effects, the first problem includes a duct and the second problem includes a barrier.

For the problem including a duct, the Monte Carlo FOM values calculated in the individual spatial cells are vastly improved by the use of both weight window types developed in this work. In particular, the solution estimates for the scalar flux are very noisy far from the solution when only survival biasing is used. Additionally, the angle-dependent weight window generates a slightly higher FOM in the duct region than the isotropic weight window. Similarly, for the problem including a barrier, the use of either type of weight window developed here results in a drastically more uniform particle distribution. Again, the angular weight window outperformed the isotropic weight window. Thus, from this work, we observe that

incorporating angular information into weight window generation can significantly improve Monte Carlo FOM for problems with strong geometric anisotropies.

2.2.4.3 LIFT

LIFT, the local importance function transform, was introduced by Turner and Larsen in 1997 [18, 19] as a new automatic Monte Carlo variance reduction method that closely approximates a zero-variance method through the use of biasing parameters. The LIFT method is partially based on the exponential transform, which adjusts the distance to collision such that particles traveling toward the region of interest undergo fewer collisions than particles traveling away from the region of interest. Particle weights are adjusted accordingly to keep the simulation unbiased. On top of the conventional exponential transform, the LIFT method adds in energy and angular biasing in each cell of the system.

LIFT uses scalar flux information from a deterministic adjoint solution to bias the source distribution, distance to collision, scattering angle, and energy. The adjoint scalar flux is also used to formulate weight windows. In the implementation presented, the weight windows are not angle-dependent. The authors note that, in the LIFT implementation, the angle-dependent weight windows require the use of an analytic expression for the angular flux at every boundary and collision site and that this extra computational effort does not generally yield increased efficiency for the Monte Carlo calculation that then employs the angle-dependent weight windows.

The LIFT strategy can be summarized in two steps. First, an analytic function is derived that is piecewise continuous in space and angle and approximates the adjoint solution within each energy group and spatial cell of the Monte Carlo system. Then, this approximate representation of the adjoint solution is used to transform the original forward problem into a new problem that can be solved by a Monte Carlo simulation with reduced variance. Increased accuracy in the approximation of the adjoint solution results in greater reduction of the variance, approaching zero variance in the solution when using an exact representation. The authors note that this limit is unachievable and that the algebraic cost of obtaining and using more accurate adjoint solutions must be balanced against the desired FOM.

The authors compare LIFT against AVATAR, considered to be one of the most efficient automated variance reduction techniques used in a major production code at the time of publication. The overall result stated in Reference [18] is that LIFT outperforms AVATAR in most problems. The reasons given for this are that LIFT particles have significantly shorter histories than AVATAR particles and that LIFT particles have smaller weight fluctuations than AVATAR particles and thus require less splitting and Russian roulette. It is noted, however, that the two methods perform comparably for problems where biasing is difficult (AVATAR does not use any biasing techniques other than survival biasing, which LIFT also employs in addition to its other biasing).

It is seen that the LIFT method loses its advantage over survival biasing as the scattering ratio of a given problem approaches unity. While FOM values from LIFT increase, the acceleration of the method compared to survival biasing becomes negligible [18]. In Reference

[19], numerical results and comparisons against AVATAR are presented. We will briefly summarize the results and conclusions here, focusing on results from the most complex scenario tested, as the work presented in this dissertation is concerned with three-dimensional multigroup problems.

Cooper and Larsen tested the LIFT method in combination with results from various types of deterministic solutions as well as in combination with weight windows generated from AVATAR. The most complex scenario tested was multigroup in energy and featured a concrete cube with a duct running through it. The duct was also concrete but with a lower density than the bulk material; it had the source at one end, the detector at the other end, and three bends along its path. In general, it was found that incorporating angular information into the AVATAR and LIFT solutions improved the FOM for the Monte Carlo calculation when using either code [19]. Taking this result into consideration as well as other conclusions drawn in work discussed earlier in this chapter, we move forward onto discussing the LDO equations, which will be developed and then used to incorporate angular information into Monte Carlo variance reduction parameter generation.

2.3 The Lagrange Discrete Ordinates (LDO) Equations

The Lagrange Discrete Ordinates (LDO) equations, shown in Equation 2.79, are formally the same as the classical discrete ordinates equations. The LDO equations differ from the discrete ordinates equations in how the scattering source is calculated and in the representation of the angular flux. In this section, we give a mathematical background for and a derivation of the LDO equations.

2.3.1 Mathematical Background

Prior to deriving the LDO equations, it is useful to summarize relevant material from approximation theory for functions defined on $\mathbb{S}^2$, the unit sphere in $\mathbb{R}^3$. We start by denoting the space of square integrable functions on $\mathbb{S}^2$ as $L^2(\mathbb{S}^2)$, where an orthonormal basis for $L^2(\mathbb{S}^2)$ is given by the spherical harmonic functions

$$Y_\ell^m(\theta,\varphi) = (-1)^\ell \sqrt{\frac{2\ell+1}{4\pi}\frac{(\ell-m)!}{(\ell+m)!}} P_\ell^m(\cos\theta) e^{im\varphi}. \tag{2.58}$$

Here, $\ell \geq 0$, $|m| \leq \ell$, P_ℓ^m is the associated Legendre function, and θ and φ are the polar and azimuthal components of $\mathbf{\Omega}$, respectively. For a given positive integer $L > 0$, we define the rotationally invariant subspace of the spherical harmonics, $\mathcal{H}_L$, as

$$\mathcal{H}_L = \text{span}\{Y_\ell^m : |m| \leq \ell, 0 \leq \ell \leq L\}, \tag{2.59}$$

with dimension $d_L = \dim \mathcal{H}_L = (L+1)^2$. Said differently, $\mathcal{H}_L$ is the vector space that is the intersection of all subspaces containing Y_ℓ^m; it is the set of all linear combinations of Y_ℓ^m. The space $\mathcal{H}_L$ admits a "reproducing kernel" given by

$$K(\mathbf{\Omega} \cdot \mathbf{\Omega}') = \sum_{\ell=0}^{L} \frac{2\ell+1}{4\pi} P_\ell(\mathbf{\Omega} \cdot \mathbf{\Omega}') \,, \tag{2.60}$$

where P_ℓ is the ℓ^{th} degree Legendre polynomial and K satisfies

$$f(\mathbf{\Omega}) = \int_{\mathbb{S}^2} K(\mathbf{\Omega} \cdot \mathbf{\Omega}') f(\mathbf{\Omega}') d\mathbf{\Omega}' \tag{2.61}$$

for all $f \in \mathcal{H}_L$.

Let $S = \{\mathbf{\Omega}_i\}_{i=1}^M$ be a given set of points (discrete directions) in $\mathbb{S}^2$ and assume that $M = d_L$. That is, the number of directions is equal to the dimension of the subspace $\mathcal{H}_L$. Then, the set S is said to be a fundamental system of points for $\mathcal{H}_L$ if the evaluation functionals

$$f \mapsto f(\mathbf{\Omega}_i), \quad i = 1, 2, \ldots, M, \quad f \in \mathcal{H}_L \tag{2.62}$$

are linearly independent. Using a spherical harmonics basis for $\mathcal{H}_L$, this is equivalent to requiring that the interpolation matrix $\mathbf{Y}$, shown in Equation 2.63, be nonsingular.

$$\mathbf{Y} = \begin{pmatrix} Y_0^0(\mathbf{\Omega}_1) & Y_0^0(\mathbf{\Omega}_2) & Y_0^0(\mathbf{\Omega}_3) & \ldots & Y_0^0(\mathbf{\Omega}_M) \\ Y_1^{-1}(\mathbf{\Omega}_1) & Y_1^{-1}(\mathbf{\Omega}_2) & & & \\ Y_0^1(\mathbf{\Omega}_1) & & \ddots & & \vdots \\ \vdots & & & & \\ Y_L^L(\mathbf{\Omega}_1) & \ldots & & & Y_L^L(\mathbf{\Omega}_M) \end{pmatrix} \tag{2.63}$$

Fundamental systems of points can be constructed geometrically or through optimization techniques. Here, we employ fundamental systems designed using numerical techniques to maximize the logarithm of the determinant of the Gram matrix, where the Gram matrix is constructed as $\mathbf{G} = \mathbf{Y}^\dagger \mathbf{Y}$ and $\mathbf{Y}^\dagger$ is the conjugate transpose (Hermitian adjoint) of $\mathbf{Y}$. This requirement leads to well-conditioned interpolation matrices. With the fundamental system of points $\{\mathbf{\Omega}_i\}_{i=1}^{d_L}$, Lagrange functions on the sphere can be defined such that

$$L_i(\mathbf{\Omega}_j) = \delta_{i,j}, \quad i, j = 1, 2, \ldots, d_L. \tag{2.64}$$

These functions $\{L_i\}_{i=1}^{d_L}$ then form a basis for $\mathcal{H}_L$. Next, we define another set of functions

$$K_i(\mathbf{\Omega}) \equiv K(\mathbf{\Omega} \cdot \mathbf{\Omega}_i), \quad i = 1, 2, \ldots, d_L. \tag{2.65}$$

Using Equations 2.62 and 2.65, the Lagrange functions and the reproducing kernel functions are related by

$$\int_{\mathbb{S}^2} L_i(\mathbf{\Omega}) K(\mathbf{\Omega}_j \cdot \mathbf{\Omega}) d\mathbf{\Omega} = \langle L_i, K_j \rangle = L_i(\mathbf{\Omega}_j) = \delta_{i,j}, \quad i,j = 1,2,\ldots,d_L. \tag{2.66}$$

This indicates that $\{K_i\}_{i=1}^{d_L}$ and $\{L_i\}_{i=1}^{d_L}$ form bi-orthogonal bases for the subspace $\mathcal{H}_L$ and so one basis can be written in terms of the other:

$$L_i(\mathbf{\Omega}) = \sum_{j=1}^{d_L} \langle L_i, L_j \rangle K_j(\mathbf{\Omega}), \tag{2.67}$$

$$K_j(\mathbf{\Omega}) = \sum_{i=1}^{d_L} \langle K_i, K_j \rangle L_i(\mathbf{\Omega}). \tag{2.68}$$

Now, define the $d_L \times d_L$ matrix $\mathbf{L}$ with elements $(\mathbf{L})_{i,j} = \langle L_i, L_j \rangle$. Using the addition theorem, the Gram matrix $\mathbf{G} = \mathbf{Y}^\dagger \mathbf{Y}$ then has the elements $(\mathbf{G})_{i,j} = K(\mathbf{\Omega}_i \cdot \mathbf{\Omega}_j) = \langle K_i, K_j \rangle$. Equations 2.67 and 2.68 imply that $\mathbf{LG} = \mathbf{I}$, where $\mathbf{I}$ is the $d_L \times d_L$ identity matrix. As mentioned previously, by the construction of the extremal point systems, the Gram matrix is well-conditioned and so the matrix elements $\langle L_i, L_j \rangle = (\mathbf{G}^{-1})_{i,j}$ can be computed accurately. Additionally, the reproducing kernel can be easily calculated using the three-term recursion relation for Legendre polynomials, so Equation 2.67 gives a convenient way to calculate the necessary Lagrange functions.

Using this framework, for any $f \in \mathcal{H}_L$,

$$f(\mathbf{\Omega}) = \sum_{i=1}^{d_L} f(\mathbf{\Omega}_i) L_i(\mathbf{\Omega}) \tag{2.69}$$

and so we can define a quadrature on $\mathcal{H}_L$ by

$$\begin{aligned} \int_{\mathbb{S}^2} f(\mathbf{\Omega}) d\mathbf{\Omega} &= \sum_{i=1}^{d_L} \int_{\mathbb{S}^2} f(\mathbf{\Omega}_i) L_i(\mathbf{\Omega}) d\mathbf{\Omega} \\ &= \sum_{i=1}^{d_L} w_i f(\mathbf{\Omega}_i), \end{aligned} \tag{2.70}$$

where

$$w_i = \int_{\mathbb{S}^2} L_i(\mathbf{\Omega}) d\mathbf{\Omega} = \sum_{j=1}^{d_L} \langle L_i, L_j \rangle. \tag{2.71}$$

In summary, the $\mathcal{H}_L$ subspace has three different basis sets: the spherical harmonics, the reproducing kernel functions, and the Lagrange functions. For the reproducing kernel

functions and the Lagrange functions to be a basis, it is required that the number of directions be equal to the dimension of the subspace. That is to say, for a Lagrange or reproducing kernel basis to exist, the number of quadrature points must be $(L+1)^2$. This is what precludes many commonly-used quadrature sets from generating a Lagrange basis and is why extremal point systems and corresponding positive weight quadratures are used here. Next, we will continue with the derivation of the LDO equations.

2.3.2 Derivation of the LDO Equations

With the appropriate mathematical background in place, we will now derive the LDO equations, keeping in mind that the end results is a set of equations that are formally the same as the discrete ordinates equations. First, we define

$$\psi_L(\mathbf{r}, E, \mathbf{\Omega}) = \sum_{n=1}^{N} \psi^n(\mathbf{r}, E) L_n(\mathbf{\Omega}), \tag{2.72}$$

where, again, $L_n(\mathbf{\Omega})$ is the n^{th} Lagrange element and N is the dimension of the rotationally invariant subspace of the spherical harmonics as defined in Equation 2.59. The coefficients $\psi^n(\mathbf{r}, E)$ will be determined through collocation. Equation 2.72 is then substituted into the NTE:

$$\mathbf{\Omega} \cdot \nabla \psi_L(\mathbf{r}, E, \mathbf{\Omega}) + \Sigma_t(\mathbf{r}, E)\psi_L(\mathbf{r}, E, \mathbf{\Omega}) = \int_0^\infty \int_{\mathbb{S}^2} \Sigma_s(\mathbf{r}, E' \to E, \mathbf{\Omega}' \cdot \mathbf{\Omega}) \psi_L(\mathbf{r}, E', \mathbf{\Omega}') d\mathbf{\Omega}' dE' + Q(\mathbf{r}, E, \mathbf{\Omega}). \tag{2.73}$$

Next, we define the residual

$$r_L(\mathbf{r}, E, \mathbf{\Omega}) \equiv \mathbf{\Omega} \cdot \nabla \psi_L(\mathbf{r}, E, \mathbf{\Omega}) + \Sigma_t(\mathbf{r}, E)\psi_L(\mathbf{r}, E, \mathbf{\Omega}) - \int_0^\infty \int_{\mathbb{S}^2} \Sigma_s(\mathbf{r}, E' \to E, \mathbf{\Omega}' \cdot \mathbf{\Omega}) \psi_L(\mathbf{r}, E', \mathbf{\Omega}') d\mathbf{\Omega}' dE' - Q(\mathbf{r}, E, \mathbf{\Omega}). \tag{2.74}$$

The energy variable is discretized with a standard multigroup approach as is done in the discrete ordinates equations:

$$r_L^g(\mathbf{r}, \mathbf{\Omega}) = \mathbf{\Omega} \cdot \nabla \psi_L^g(\mathbf{r}, \mathbf{\Omega}) + \Sigma_t^g(\mathbf{r})\psi_L^g(\mathbf{r}, \mathbf{\Omega}) - \sum_{g'=0}^{G-1} \int_{\mathbb{S}^2} \Sigma_s^{g' \to g}(\mathbf{r}, \mathbf{\Omega}' \cdot \mathbf{\Omega}) \psi_L^{g'}(\mathbf{r}, \mathbf{\Omega}') d\mathbf{\Omega}' - Q^g(\mathbf{r}, \mathbf{\Omega}), \quad g = 0, 1, \ldots, G-1. \tag{2.75}$$

Next, the scattering integral is evaluated analytically. In this evaluation, we suppress energy dependence for brevity.

$$\begin{aligned}
\int_{\mathbb{S}^2} \Sigma_s(\mathbf{r}, \boldsymbol{\Omega}' \cdot \boldsymbol{\Omega}) \psi_L(\mathbf{r}, \boldsymbol{\Omega}') d\boldsymbol{\Omega}' &= \int_{\mathbb{S}^2} \Sigma_s(\mathbf{r}, \boldsymbol{\Omega}' \cdot \boldsymbol{\Omega}) \sum_{n=1}^{N} \psi^n(\mathbf{r}) L_n(\boldsymbol{\Omega}') d\boldsymbol{\Omega}' \\
&= \sum_{n=1}^{N} \psi^n(\mathbf{r}) \int_{\mathbb{S}^2} \Sigma_s(\mathbf{r}, \boldsymbol{\Omega}' \cdot \boldsymbol{\Omega}) L_n(\boldsymbol{\Omega}') d\boldsymbol{\Omega}' \\
&= \sum_{n=1}^{N} \psi^n(\mathbf{r}) \int_{\mathbb{S}^2} \Sigma_s(\mathbf{r}, \boldsymbol{\Omega}' \cdot \boldsymbol{\Omega}) \sum_{m=1}^{N} \langle L_n, L_m \rangle K_m(\boldsymbol{\Omega}') d\boldsymbol{\Omega}' \\
&= \sum_{n=1}^{N} \psi^n(\mathbf{r}) \sum_{m=1}^{N} \langle L_n, L_m \rangle \int_{\mathbb{S}^2} \Sigma_s(\mathbf{r}, \boldsymbol{\Omega}' \cdot \boldsymbol{\Omega}) K_m(\boldsymbol{\Omega}') d\boldsymbol{\Omega}' \\
&= \sum_{n=1}^{N} \psi^n(\mathbf{r}) \sum_{m=1}^{N} \langle L_n, L_m \rangle \Sigma_{s,L}(\mathbf{r}, \boldsymbol{\Omega}_m \cdot \boldsymbol{\Omega}).
\end{aligned} \tag{2.76}$$

Here, the reproducing property of the function K was used and $\Sigma_{s,L}(\mathbf{r}, \boldsymbol{\Omega}_m \cdot \boldsymbol{\Omega})$ denotes the scattering cross section restricted to maximum degree L [20]. It is assumed that total and absorption group cross sections are independent of angle. Equations 2.72 and 2.76 are then substituted into the residual expression:

$$\begin{aligned}
r_L^g(\mathbf{r}, \boldsymbol{\Omega}) = \\
&\boldsymbol{\Omega} \cdot \sum_{n=1}^{N} \left[\nabla \psi^{g,n}(\mathbf{r})\right] L_n(\boldsymbol{\Omega}) + \Sigma_t^g(\mathbf{r}) \sum_{n=1}^{N} \psi^{g,n}(\mathbf{r}) L_n(\boldsymbol{\Omega}) \\
&- \sum_{g'=0}^{G-1} \sum_{n'=1}^{N} \sum_{m=1}^{N} \langle L_{n'}, L_m \rangle \Sigma_{s,L}^{g' \to g}(\mathbf{r}, \boldsymbol{\Omega}_m \cdot \boldsymbol{\Omega}) \psi^{g',n'}(\mathbf{r}) \\
&\qquad - Q^g(\mathbf{r}, \boldsymbol{\Omega}).
\end{aligned} \qquad g = 0, 1, \ldots, G-1. \tag{2.77}$$

Next, the collocation procedure requires the residual to be zero at the points $\{\boldsymbol{\Omega}_n\}_{n=1}^N$. This leads to the $G \times N$ equations

$$\begin{aligned}
&\boldsymbol{\Omega}_n \cdot \nabla \psi^{g,n}(\mathbf{r}) + \Sigma_t^g(\mathbf{r}) \psi^{g,n}(\mathbf{r}) = \\
&\sum_{g'=0}^{G-1} \sum_{m=1}^{N} \sum_{n'=1}^{N} \langle L_{n'}, L_m \rangle \Sigma_{s,L}^{g' \to g}(\mathbf{r}, \boldsymbol{\Omega}_m \cdot \boldsymbol{\Omega}_n) \psi^{g',n'}(\mathbf{r}) + Q^{g,n}(\mathbf{r}),
\end{aligned} \qquad \begin{array}{l} g = 0, 1, \ldots, G-1, \\ n = 1, 2, \ldots, N. \end{array} \tag{2.78}$$

In the collocation procedure, we have made use of the interpolation property of the Lagrange functions, i.e. $L_a(\boldsymbol{\Omega}_b) = \delta_{a,b}$.

Finally, we discretize the spatial variable in the same way as was done for the discrete ordinates equations, giving the $G \times I \times J \times K \times N$ multigroup LDO equations:

$$\begin{aligned} \boldsymbol{\Omega}_n \cdot \nabla \psi^{g,n}_{i,j,k} + \Sigma^{g}_{t,i,j,k} \psi^{g,n}_{i,j,k} = & \\ \sum_{g'=0}^{G-1} \sum_{m=1}^{N} \sum_{n'=1}^{N} \langle L_{n'}, L_m \rangle \Sigma^{g' \to g}_{s,L,i,j,k} (\boldsymbol{\Omega}_m \cdot \boldsymbol{\Omega}_n) \psi^{g',n'}_{i,j,k} + Q^{g,n}_{i,j,k}, & \end{aligned} \quad \begin{aligned} & g = 0, 1, \ldots, G-1, \\ & i = 1, 2, \ldots, I, \\ & j = 1, 2, \ldots, J, \\ & k = 1, 2, \ldots, K, \\ & n = 1, 2, \ldots, N. \end{aligned} \tag{2.79}$$

Here, N is the number of discrete angles used in the formulation and is a property of the maximum degree of integration of the quadrature set on which the equations are based, L_n is the n^{th} Lagrange function, and $\Sigma_{s,L}$ is the scattering cross section restricted to maximum degree L.

The difference in how the scattering source is calculated between Equations 2.17 and 2.79 has important implications, which we will explore in Chapter 3. The most apparent difference is that the LDO equations do not require the calculation of spherical harmonic moments of the angular flux. It is also important to note that the extremal point systems on which the LDO equations are based do not possess symmetries like those of the commonly-used quadrature sets discussed earlier.

The LDO formulation has never before been implemented in a full-scale radiation transport framework, nor has it been studied in the context of Monte Carlo variance reduction parameter generation. The following chapter will discuss the implementation of the LDO equations in the Exnihilo software package as well as the methodology employed for using the equations' solutions in automated Monte Carlo variance reduction parameter generation.

Bibliography

[1] E.E. Lewis and W.F. Miller. *Computational Methods of Neutron Transport*. New York, NY: John Wiley & Sons, Inc., 1984.

[2] X-5 Monte Carlo Team. *MCNP – A General Monte Carlo N-Particle Transport Code, Version 5*. Volume I: Overview and Theory. LA-UR-03-1987. Revised 2/1/2008. Los Alamos National Laboratory, Los Alamos, NM, Apr. 2003. URL: https://laws.lanl.gov/vhosts/mcnp.lanl.gov/pdf_files/la-ur-03-1987.pdf.

[3] Richard H. Olsher. "A Practical Look at Monte Carlo Variance Reduction Methods in Radiation Shielding". In: *Nuclear Engineering and Technology* 38.3 (2006), pp. 225–230.

[4] Cory D. Ahrens. "Lagrange Discrete Ordinates: A New Angular Discretization for the Three-Dimensional Linear Boltzmann Equation". In: *Nuclear Science and Engineering* 180.3 (2015), pp. 273–285.

[5] Thomas Evans et al. *Exnihilo Transport Methods Manuals*. Tech. rep. CASL-U-2015-0080-000, Revision 0. Oak Ridge National Laboratory, Mar. 2015.

[6] Thomas M. Evans et al. "Denovo: A new three-dimensional parallel discrete ordinates code in SCALE". In: *Nuclear Technology* 171.2 (2010), pp. 171–200. URL: https://doi.org/10.13182/NT171-171.

[7] S.W. Mosher et al. *ADVANTG – An Automated Variance Reduction Parameter Generator*. Tech. rep. ORNL/TM-2013/416, Rev. 1. Oak Ridge National Laboratory, Aug. 2015.

[8] Kaye D. Lathrop. "Ray Effects in Discrete Ordinates Equations". In: *Nuclear Science and Engineering* 32.3 (1968), pp. 357–369.

[9] Ray E. Alcouffe et al. *PARTISN: A Time-Dependent, Parallel Neutral Particle Transport Code System*. Tech. rep. LA-UR-05-3925. Los Alamos National Laboratory, May 2005.

[10] John C. Wagner and Alireza Haghighat. "Automated Variance Veduction of Monte Carlo Shielding Calculations using the Discrete Ordinates Adjoint Function". In: *Nuclear Science and Engineering* 128.2 (1998), pp. 186–208.

[11] John C. Wagner, Edward D. Blakeman, and Douglas E. Peplow. "Forward-weighted CADIS Method for Variance Reduction of Monte Carlo Calculations of Distributions and Multiple Localized Quantities". In: *Proceedings of the 2009 Int. Conference on Advances in Mathematics, Computational Methods, and Reactor Physics, Saratoga Springs, NY*. 2009.

[12] Douglas E. Peplow, Scott W. Mosher, and Thomas M. Evans. *Consistent Adjoint Driven Importance Sampling using Space, Energy, and Angle*. Tech. rep. ORNL/TM-2012/7. Oak Ridge National Laboratory, 2012.

[13] M. Munk et al. "FW/CADIS-Ω: An angle-informed hybrid method for deep-penetration radiation transport". In: *Proceedings of the PHYSOR 2016 Meeting in Sun Valley, ID* (May 2016). URL: https://arxiv.org/pdf/1612.00793.pdf.

[14] Madicken Munk. "FW/CADIS-Ω: An Angle-Informed Hybrid Method for Neutron Transport". PhD thesis. University of California, Berkeley, 2017.

[15] Kenneth A. Van Riper et al. "AVATAR – Automatic variance reduction in Monte Carlo calculations". In: *Proceedings of the Joint International Conference on Mathematical Methods & Supercomputing for Nuclear Applications in Saratoga Springs, NY* (October 1997). URL: http://www.osti.gov/scitech/biblio/527548.

[16] Raymond E. Alcouffe. *THREEDANT: A Code To Perform Three-Dimensional, Neutral Particle Transport Calculations*. Tech. rep. LA-UR-94-3259. Los Alamos National Laboratory, 1994.

[17] Marc A. Cooper and Edward W. Larsen. "Automated weight windows for global Monte Carlo particle transport calculations". In: *Nuclear science and engineering* 137.1 (2001), pp. 1–13. URL: http://www.ans.org/pubs/journals/nse/a_2171.

[18] Scott A. Turner and Edward W. Larsen. "Automatic variance reduction for three-dimensional Monte Carlo simulations by the local importance function transform-I: Analysis". In: *Nuclear Science and Engineering* 127.1 (1997), pp. 22–35. URL: https://doi.org/10.13182/NSE127-22.

[19] Scott A. Turner and Edward W. Larsen. "Automatic variance reduction for three-dimensional Monte Carlo simulations by the local importance function transform-II: Numerical Results". In: *Nuclear Science and Engineering* 127.1 (1997), pp. 36–53. URL: https://doi.org/10.13182/NSE127-36.

[20] C.D. Ahrens. *Derivation of New 3D Discrete Ordinate Equations*. Tech. rep. American Nuclear Society, Inc., 555 N. Kensington Avenue, La Grange Park, Illinois 60526 (United States), 2012.